Kagome quantum spin systems in the atacamite family

Pascal Puphal,[1] Katharina M. Zoch,[1] Joy Désor,[1] Michael Bolte,[2] and Cornelius Krellner[1]
[1]*Physikalisches Institut, Goethe-Universität Frankfurt, 60438 Frankfurt am Main, Germany*
[2]*Institut für Organische Chemie der Universität Frankfurt, 60439 Frankfurt am Main, Germany*

(Received 18 April 2018; revised manuscript received 30 May 2018; published 29 June 2018)

We present the hydrothermal synthesis, as well as structural and chemical analysis, of single crystals of $EuCu_3(OH)_6Cl_3$, $Zn_xCu_{4-x}(OH)_6(NO_3)_2$ and haydeeite, and $MgCu_3(OH)_6Cl_2$ compounds, all arising from the atacamite family. Magnetic and specific-heat measurements down to 1.8 K are carried out for these systems. $EuCu_3(OH)_6Cl_3$ has a frustrated antiferromagnetic Cu^{2+} ground state with order at 15 K, and a strong anisotropy and increased magnetization from Van Vleck paramagnetic Eu^{3+} contributions. $ZnCu_3(OH)_6(NO_3)_2$ reveals antiferromagnetic order at 9 K and measurements on haydeeite single crystals confirm the ferromagnetic order at 4.2 K with the easy axis within the kagome plane. These results prove that the atacamite family presents a broad class of materials with interesting magnetic ground states.

DOI: 10.1103/PhysRevMaterials.2.063402

I. INTRODUCTION

The discovery of the first reported prototype with magnetic Cu^{2+} ions arranged on a kagome layer presenting a quantum spin liquid (QSL [1]) in herbertsmithite [$ZnCu_3(OH)_6Cl_2$] [2] triggered enormous interest for this novel ground state. The dominant Cu-O-Cu antiferromagnetic superexchange of $J = -197$ K [3] in the kagome plane is strongly frustrated due to the geometrical arrangement of the ions. Considering the possibility of variable Zn for Cu substitution in $Zn_xCu_{4-x}(OH)_6Cl_2$, one can influence the magnetic properties of the compounds: increasing the Zn concentration in between these kagome layers leads to their magnetic decoupling and thus to a suppression of the magnetic order [4]. For the composition $ZnCu_3(OH)_6Cl_2$ ($x = 1$), no magnetic long-range order is registered down to $T = 50$ mK [3]. Later on, it has been realized that some Zn-Cu antisite disorder (up to 15% in terms of occupation parameters) is always present in herbertsmithite [5,6], which has led to the search for further kagome materials, with less amount of structural disorder. The atacamite family of compounds presents a rich field of different substitution possibilities [7] based on the three basic polymorphs of $Cu_2(OH)_3Cl$: atacamite, clinoatacamite and botallackite, allowing substitutions both on the Cu and Cl place. Cationic substitutions would dilute the concentration of Cu^{2+} ions between and in the kagome planes, while those on the anionic sites would have a direct impact on the spatial separation of these active planes. Furthermore, it was proposed that substituting trivalent ions on the divalent Zn/Cu ions will lead to a correlated Dirac-kagome metal combining Dirac electrons, strong interactions, and frustrated magnetism [8]. However, experimentally, it was found that the structure presents charge balancing with additional Cl^- rather than electron doping, as seen for the nonmagnetic Y [9,10] and the magnetic Nd, Gd, and Sm [11] ions.

In Table I, we present the whole class of $M_xCu_{4-x}(OH)_6X_2$, where M represents a divalent ion and X a halide, nitrate or sulfate, with detailed information on the structure type and magnetism. The atom type of substitution is highlighted by a color and its crystal ionic radius is given in the fourth column. The given space group in the fifth column enables a division into two main structural variants: the herbertsmithite $R\bar{3}m$ type structure containing ABC stacked kagome layers with intermediate layers of the substituent and the kapellasite type with AA stacked layers, where the substituent is in the kagome layer in the center of the star (see Fig. 2). Other groups are the basic structures with possible substitutions on the halide site, then the crossover paratacamite over herbertsmithite to the substitutions of $x = 2$ leading with nonmagnetic ions to one-dimensional chain systems, and finally the $x = 4$ entirely substituted variants. The last type shows the structural variance of this family and the possibility of undescribed intermediate candidates. We want to highlight the work of Ref. [12], which already shows a rich amount of variants only for the $M_2(OH)_3$(Cl,Br,I) candidates. Besides the shown atacamite type, a "kapellasite-type" structure called α variant was found by Oswald and Feitknecht [12] for Co, Ni, Mg, Fe, Mn with $x = 4$ substitution. As well as paratacamite variants of Co/ Fe and botallackite types for Br/I both for Cu, Co, Ni, Fe as well as Mn.

The columns (6–9) give details about the magnetic properties and are followed by some structural details of the Cu ions (10–12), where Cu_K stands for the shortest copper distances in the kagome plane and Cu_{inter} for the distances between these layers ignoring Cu atoms in between. The column number 12 contains the bonding angle of Cu-O-Cu where the largest and thus dominating J is chosen. In the last two columns, references are given. So far, the only kagome systems of this family presenting no magnetic order down to mK temperatures are both $ZnCu_3(OH)_6Cl_2$ herbertsmithite and kapellasite, $ZnCu_3(OH)_6FBr$, called Zn-barlowite, and $MgCu_3(OH)_6Cl_2$ tondiite, which all have a strong Zn-Cu or Mg-Cu exchange. Other quantum spin liquid candidates of the family are ones presenting isolated trimers found in $SrCu(OH)_3Cl$ [13] and $ZnCu_3(OH)_6SO_4$ [14], which so far only exist as polycrystals.

TABLE I. List of the atacamite family divided into four classes of structures each sorted by the size of the substitution ions. The table includes the mineral name if naturally existing, the chemical formula, the 6 fould coordinated radius of the substituted ion, the structural space group, the lattice type of the magnetic ion (K: kagome, P: pyrochlore, T: triangular and 1D: chains), the magnetic transition temperature, the Curie-Weiss temperature with the resulting frustration as well as the Cu arrangements. Column 10–12 describe the structure with first the relevant magnetic ion distance, then the distance between the sought kagome layers (ignoring the position in between) and finally the highest Cu-O-Cu bonding angle. In the next-to-last column first the reference for the magnetic properties is given, then the one of the structure and in the last column a reference for single crystal growth. If the substitution ion itself is magnetic the whole line is written in italic.

Type	Mineral name	Formula	r [pm] [15–17]	Point group	Magnetic lattice	Magnetic order [K]	Θ_W [K]	f	Cu_K [Å]	Cu_{inter} [Å]	∠(Cu1-O1 –Cu1) [°]	Reference (mag, struc)	sc growth
parent	atacamite	$Cu_2(OH)_3Cl$	72	Pnma	P	9	–125	14	3.432	5.464	124.39	[18]	–
	clinoatacamite	$Cu_2(OH)_3Cl$	72	$P2_1/n$	P	6.5	–200	30	3.410	5.023	120.21	[19]	[20]
	botallackite	*(Ni/Co/Fe/Mn/Cu)*$_2$-$(OH)_3$(Cl/Br/I)	*69/ 74.5/ 75/ 83* 172/ 188/ 210	*$P2_1/m$*	*T*	*7.2/10/14*	*0.41*	*0*	*3.059*	*5.716*	*107.91*	[12,18]	–
"herbertsmithite-type"	brochantite	$Cu_4(OH)_6SO_4$	258	$P2_1/n$	'1D'	6.3	–90	14	3.005	5.062	124.5	[21]	–
	rouaite	$Cu_2(OH)_3(NO_3)$	179	$P2_1$	T	11	–12	1	3.05	6.929	110.33	[22,23]	–
	claringbullite	$Cu_4(OH)_6ClF$	126	$P6_3/mmc$	P	17	–33	2	3.337	2.737	117.56	[22,24]	–
	barlowite	$Cu_4(OH)_6BrF$	188, 126	$P6_3/mmc$	P	15	–136	9	3.339	2.757	117.21	[25,26]	[27]
	paratacamite	$Zn_xCu_{4-x}(OH)_6Cl_2$	73	$R\bar{3}m$	K	6	–231	38.5	3.416	3.110	122.28	[2,28] $x = 0.5/0.25$	[20]
	–	$Ga_{0.8}Cu_{3.2}(OH)_6Cl_2$	62	$R\bar{3}m$	K	5	–256	55	3.421	5.066	118.88	[29]	–
	gillardite	*$NiCu_3(OH)_6Cl_2$*	*69*	*$R\bar{3}m$*	*K*	*6*	*–100*	*17*	*3.418*	*5.020*	*119.19*	[30,31]	–
	tondiite	$MgCu_3(OH)_6Cl_2$	72	$R\bar{3}m$	K	–	–300	∞	3.416	5.054	119.05	[32]	[32]
	herbertsmithite	$ZnCu_3(OH)_6Cl_2$	73	$R\bar{3}m$	K	–	–300	∞	3.416	5.087	118.92	[2,33]	[20]
	–	$ZnCu_3(OH)_6BrF$	73, 188, 126	$P6_3/mmc$	K	–	–205	∞	3.337	4.660	117.01	[34]	–
"kapellasite-type"	*leverettite*	*$CoCu_3(OH)_6Cl_2$*	*74.5*	*$R\bar{3}m$*	*K*	*3*	*–40*	*13*	*3.421*	*5.096*	*119.19*	[30,35]	–
	–	*$CdCu_3(OH)_6Cl_2$*	*95*	*$P2_1/n$*	*K*	–	*–150*	*75*	*3.015*	*5.758*	*108.50*	[36]	–
	haydeeite	$MgCu_3(OH)_6Cl_2$	72	$P\bar{3}m1$	K	4.3 (FM)	28	7	3.137	5.750	104.98	[37,38]	this paper
	kapellasite	$ZnCu_3(OH)_6Cl_2$	73	$P\bar{3}m1$	K	–	9,5	∞	3.150	5.733	105.84	[37,39]	–
	–	$ZnCu_3(OH)_6(NO_3)_2$	73, 179	$P2_1$	K?	7.5	0	0	3.065	6.927	104.07	this paper	this paper
	misakiite	*$MnCu_3(OH)_6Cl_2$*	*83*	*$P\bar{3}m1$*	*T*	*10*	*–25*	*3*	*3.208*	*5.710*	*108.00*	[40]	–
	–	$YCu_3(OH)_6Cl_3$	90	$P\bar{3}m1$	K	12	–100	8.33	3.250	5.618	117.36	[10]	–
	–	$Y_3Cu_9(OH)_{19}Cl_8$	90	$R\bar{3}$	K	2.2	–100	45	3.250	5.679	117.47	[9]	[9]
	–	$EuCu_3(OH)_6Cl_3$	94.7	$P\bar{3}m1$	K	15	–400	119.3	3.418	5.630	119.34	this paper	this paper
	–	*$CdCu_3(OH)_6(NO_3)_2$*	*95, 179*	*$P\bar{3}m1$*	*K*	*4*	*45*	*11*	*3.261*	*7.012*	*106.43*	[22,41]	[41]
	–	*$SmCu_3(OH)_6Cl_3$*	*95.8*	*$P\bar{3}m1$*	*T*	*18*	*–106*	*5*	*3.432*	*5.639*	*120.1*	[11]	–
	–	*$NdCu_3(OH)_6Cl_3$*	*98.3*	*$P\bar{3}m1$*	*T*	*20*	*–345*	*19*	*3.411*	*5.625*	*119.30*	[11]	–
$x = 2$	centennialite	$CaCu_3(OH)_6Cl_2$	100	$P\bar{3}m1$	K	5	–56	11	3.324	5.760	114.09	[42]	[43]
	–	$ZnCu(OH)_3Cl$	73	$P2_1/m$	1D	?	?	?	3.195	5.688	107.70	[44]	–
	iyoite	*$MnCu(OH)_3Cl$*	*83*	*$P2_1/m$*	*1D*	*29*	*–80*	*3*	*3.302*	*5.721*	*114.12*	[40]	–
trimer	–	$SrCu(OH)_3Cl$	117	$Pmn2_1$	Trimer	–	–135	∞	3.395	6.972	119.40	[13]	–
	–	$ZnCu_3(OH)_6SO_4$	73, 258	$P2_1/a$	Trimer	–	–79	∞	2.781	4.441	91.86	[14]	–
$x = 4$	"*atacamite*"	*$(Ni/Mg/Mn)_2(OH)_3Cl$*	*69/ 72/ 83*	*Pnma*	*P*	*5/3.4*	*–100/-57.8*	*20/17*	*3.359*	*5.190*	*107.7*	[12,45,46]	–
	"*kapellasite*"	*$(Ni/Co/Mg/Fe/Mn)_2(OH)_3Cl$*	*69/ 74.5/ 75/72/ 83*	*$P\bar{3}m1$*	*T*	?	?	?	?	?	?	[12]	–

In addition to these compounds, we present another example of the $P\bar{3}m1$ structure with a trivalent Eu^{3+} ion realized in $EuCu_3(OH)_6Cl_3$. As well as an example of an antiferromagnetic system with no strong frustration effects, observed in $ZnCu_3(OH)_6(NO_3)_2$ and the successful single-crystal growth of the ferromagnetic haydeeite $MgCu_3(OH)_6Cl_2$.

II. EXPERIMENTAL DETAIL

For the single-crystal growth, a hydrothermal Parr 4625 autoclave with a 575 ml filling capacity operated by a Parr 4842 power supply including a 982 Watlow controller was used.

The energy dispersive x-ray spectra (EDS) were recorded with an AMETEK EDAX Quanta 400 detector in a Zeiss DSM 940A scanning electron microscope (SEM). A layer of carbon was sputtered on the isolating single crystals using a Balzers Union FL-9496.

X-ray powder diffraction data were collected on a Bruker D8 Focus using a Cu x-ray generator and the Rietveld refinement of the x-ray data was done using the fullprof suite [47]. For the single-crystal structure determination, the data were collected at 173 K on a STOE IPDS II two-circle diffractometer with a Genix Microfocus tube with mirror optics using Mo K_α radiation ($\lambda = 0.71073$ Å). The data were scaled using the frame scaling procedure in the X-AREA program system [48]. The structure was solved by direct methods using the program SHELXS [49] and refined against F^2 with full-matrix least-squares techniques using the program SHELXL-97 [49]. The H atoms bonded to O were found in a difference map and was isotropically refined with the O-H distances restrained to 0.84(1) Å.

The specific-heat and magnetic measurements were collected with the standard options of a Physical Property Measurement System from Quantum Design in a temperature range of 1.8 to 350 K.

III. $EuCu_3(OH)_6Cl_2$

A. Synthesis

Single crystals of $EuCu_3(OH)_6Cl_3$ were prepared in the Parr autoclave with a temperature profile adapted from the optimized one for $Y_3Cu_9(OH)_{19}Cl_8$ [9]. For the crystallization, we prepared duran glass ampoules as follows: the ampoules were loaded with 0.6513 g CuO and 2 g $EuCl_3 \cdot 6H_2O$, solved in 5 ml distilled water and then sealed at air. They were placed in the autoclave, which was filled with distilled water to ensure the same pressure as in the ampoules. The autoclave was heated up to 270 °C in four hours and subsequently cooled down to 170 °C with 1 K/h, followed by a fast cooling to room temperature. Afterwards, the ampoules were opened and the content was filtered with distilled water. The ampoules contained a few larger single crystals, some smaller ones, and a pellet. The crystals have blue color and a hexagonal shape with typical sizes up to $1 \times 1 \times 0.25$ mm^3 [see Fig. 2(c)]. Similar to $Y_3Cu_9(OH)_{19}Cl_8$ [9] and haydeeite, the crystal habitus gives information about all crystallographic axis, with the a and b axes being the corners of the hexagon and the c axis perpendicular to the surface of the platelets. Attempts with lower and higher $EuCl_3 \cdot 6H_2O$ content in the solutions were also successful but led to smaller single crystals. However, the Eu content does not change with varying salt amount, which was deduced from EDS.

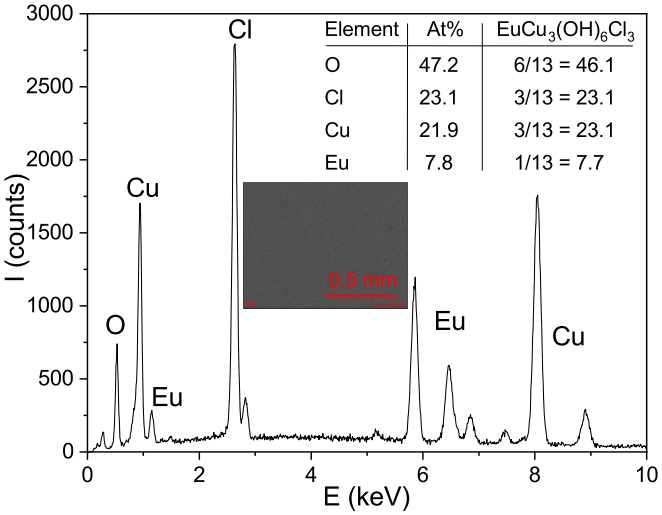

FIG. 1. EDS analysis on a polished single crystal of $EuCu_3(OH)_6Cl_3$. In a table, the measured at% are given compared to the stoichiometric values, not including the H atoms. The inset shows a SEM image, which would have shown impurity phases as grey-scaled contrast, proving the homogeneity of the crystal.

Furthermore, a growth in an external temperature gradient similar to [50] led to large single crystals of up to $2 \times 2 \times 0.75$ mm^3 [shown in Fig. 2(b)]. We used 2 g pre-reacted $EuCu_3(OH)_6Cl_3$ in a solution of 1 g $EuCl_3 \cdot 6H_2O$ with 5 ml H_2O sealed in a thick walled quartz ampoule of 15 cm length. Then we placed this ampoule into an external gradient of 2 °C/cm, with 250 °C at the hot end and 220 °C at the cold end. After several weeks the whole powder was recrystallized.

B. EDS Analysis

We measured EDS in the SEM on several crystals of different batches both of polished and untreated single crystals. In Fig. 1, an EDS spectrum is shown with the SEM image on the inset showing a clean surface with no impurity phases. The resulting at% are given in the figure and are in overall agreement with stoichiometric values of $EuCu_3(OH)_6Cl_3$. We measured several points on many crystals of different batches and did not observe any variance regarding the Eu-Cu ratio. This is typical for the $P-3m1$ structure, which has no intermediate substitutions and no paratacamitelike crossover structure. For example, kapellasite and haydeeite [39,51] stabilizes a certain substitution amount above one. By directly comparing only the Cu/Eu ratio, we found the Eu amount, assuming $Eu_xCu_{4-x}(OH)_6Cl_3$, to be not increased with an average of $x_{Eu} = 1.01 \pm 0.01$.

C. Structure

$EuCu_3(OH)_6Cl_3$ crystallizes in the kapellasite type structure $P-3m1$ with an additional Cl position just like Y, Nd, Sm, and Gd [9–11]. The structure was obtained by single-crystal diffraction and confirmed with powder diffraction [52]. It

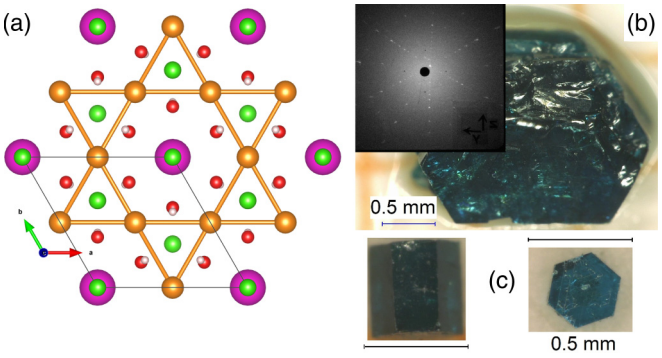

FIG. 2. (a) Image of the $P-3m1$ structure viewed onto the ab plane. There, the orange starlike kagome arrangement of the Cu atoms is apparent. The pink europium atoms are positioned in the center of the star in the kagome plane typical for the kapellasite $P-3m1$ structure. (b) Laue-image and a picture of a large $EuCu_3(OH)_6Cl_3$ crystal with a coaligned twin obtained from an external gradient growth. (c) Image of two representative untreated blue $EuCu_3(OH)_6Cl_3$ single crystals from a growth in the autoclave showing nice hexagonal shape.

is shown in Fig. 2(a) viewed along the c axis revealing the kagome star of the orange Cu atoms. The distances are $d_{\text{Cu1-Cu1}} = 3.4181(4)$ Å of the Cu atoms in the kagome plane and $d_{\text{Cu1-Cu2}} = 5.6301(13)$ Å between the AA stacked planes. The angle for the dominant superexchange is $\angle(\text{Cu1-O1-Cu1}) = 119.34(16)°$. The resulting blue crystals shown in Figs. 2(b) and 2(c) have a hexagonal shape directly revealing the structure enabling an easy orientation. The atomic positions are given in Table II.

D. Magnetic susceptibility

In this section, we present a thorough magnetic analysis on $EuCu_3(OH)_6Cl_3$ single crystals. To obtain larger masses for a reduced noise ratio, four single crystals were aligned with either the magnetic field parallel ($\|$) or perpendicular ($\perp$) to the kagome plane. We start with the analysis of the susceptibility at 9 T for temperatures between 2 and 350 K, shown in Fig. 3. In this temperature regime, Eu^{3+} ions cause pronounced Van Vleck paramagnetism, which gives a separate magnetic contribution in addition to the magnetism from the Cu^{2+}. The susceptibility in this temperature range reveals a pronounced anisotropy, $\chi_{\|}/\chi_{\perp}$ from 1.7 at 350 K to 2.5 at

TABLE II. Structural table obtained by refining single-crystal diffraction data on a $EuCu_3(OH)_6Cl_3$ single crystal measured at 173 K. A trigonal $P-3m1$ (No. 164) structure with a unit cell of $a = b = 6.8363(14)$ Å, $c = 5.6301(13)$ Å, $\alpha = \beta = 90°$, and $\gamma = 120°$ was found, where the occupation was fixed to 1.

position	x/a	y/b	z/c	Occ.	U_{iso}	Site	Sym.
Eu1	0	0	0.5	1	0.0131(3)	1b	$-3m.$
Cu1	0.5	0	0.5	1	0.0123(4)	3f	$.2/m.$
Cl1	0.666667	0.333333	0.1359(4)	1	0.0190(6)	2d	$3m.$
Cl2	0	0	0	1	0.0176(7)	1a	$-3m.$
O1	0.8066(4)	0.1934(4)	0.6318(7)	1	0.0122(8)	6i	$.m.$
H1	0.790(8)	0.210(8)	0.776(4)	1	–	6i	$.m.$

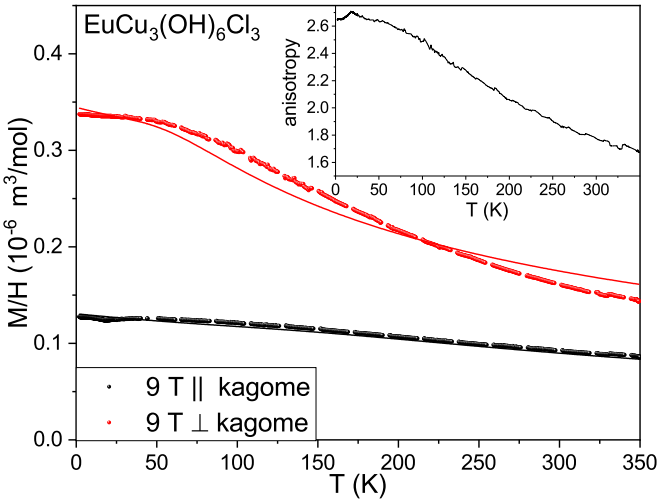

FIG. 3. The image shows the magnetic data on a stack of four single crystals with a mass of 2 mg of the temperature-dependent susceptibility data at 9 T with the field aligned (black dots) and perpendicular to the kagome plane (red dots). The line is obtained by a fit using both Van Vleck and Curie-Weiss contribution. On the inset, the temperature-dependent anisotropy of perpendicular/parallel susceptibility is shown.

50 K plotted in the inset of Fig. 3. This anisotropy is most likely attributed to the Van Vleck contribution, similar as it was observed in Ref. [53,54]. There, the anisotropy arises from a splitting of the $^1F_1$ level due to a crystal electric field. In literature, this anisotropy was analyzed for a tetragonal symmetry of the Eu^{3+}, while in $EuCu_3(OH)_6Cl_3$ the europium atoms are located on a site with hexagonal symmetry. We fitted the experimental data in the full range from 1.8 K to 350 K at a high field of 9 T in Fig. 3 with the sum of a general Van Vleck part (see Ref. [55]) and the Curie-Weiss contribution from three Cu^{2+} ions following the formula

$$\chi_{\text{mol}} = 3\frac{C}{T+\Theta_W} + \frac{N_A\mu_0\mu_B^2}{3\lambda}\left(\frac{24+\left(13.5\frac{\lambda}{k_BT}-1.5\right)e^{-\lambda/(k_BT)}+\ldots}{1+3e^{-\lambda/(k_BT)}+\ldots}\right)$$

to account for the different magnetic contributions. We note, however, that the two contributions are hard to separate and the obtained values are only an estimate, since a nonmagnetic reference, e.g., $EuZn_3(OH)_6Cl_3$ would be necessary to accurately define the Eu^{3+} Van Vleck contributions. Assuming a generally similar behavior as for the tetragonal symmetry, we get a spin-orbit value of roughly $\lambda = (2\lambda_{\|}+\lambda_{\perp})/3 = (2\times 210+586)/3$ K $= 335$ K comparable to Eu_2CuO_4 with $\lambda = 315$ cm$^{-1} \approx 300$ K [53]. The Curie-Weiss temperature was calculated in this global fit yielding roughly $\Theta_W \approx -400$ K. From a $\sqrt{\chi T}$ plot (not shown), the whole material reveals increased effective moment values of $\mu_{\text{eff}}^{\|} = 3.25\,\mu_B$ and $\mu_{\text{eff}}^{\perp} = 2.5\,\mu_B$ at 350 K compared to the theoretical one for Cu^{2+} of $1.73\,\mu_B$ as a result of the mixture with the Van Vleck contribution of Eu^{3+}.

In Fig. 4, we present the low-temperature behavior of the susceptibility of $EuCu_3(OH)_6Cl_3$, which is dominated by

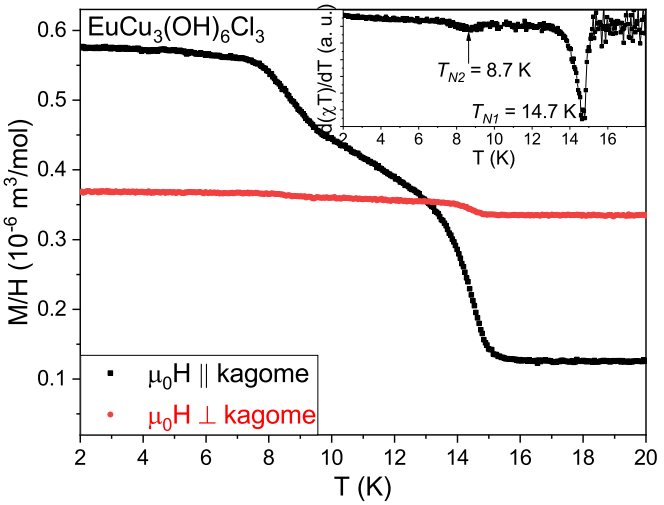

FIG. 4. The main figure shows the low-temperatue part of the susceptibility data of $EuCu_3(OH)_6Cl_3$ field cooled at 0.1 T both measured with the field aligned (red) and perpendicular to the kagome plane (black). (Inset) Derivative of χT at a tiny field of 50 Oe.

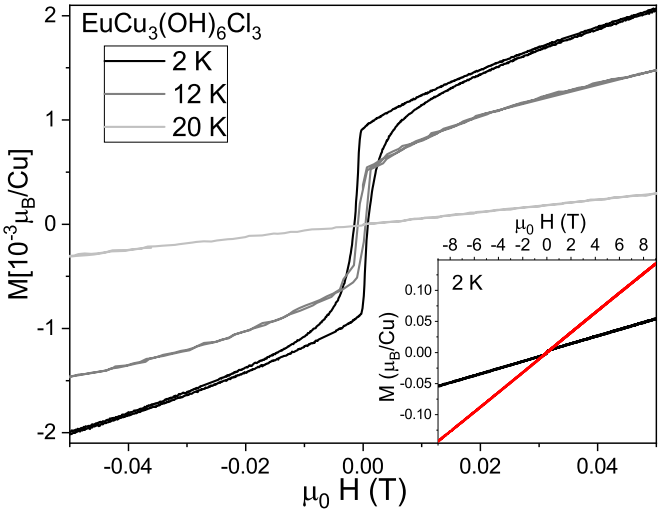

FIG. 5. Excerpt of the M(H) curves measured at 2 (black), 12 (dark grey), and 20 K (light grey) with a field applied parallel to the kagome plane. The inset shows the full range for a measurement at 2 K for both parallel (black) and perpendicular fields (red).

the Cu magnetism. Two magnetic transitions are apparent at $T_{N_1} = 14.7$ K and $T_{N_2} = 8.7$ K for both field directions. The transition temperatures can best be determined by the derivative $d(\chi T)/dT$ at very small field, shown in the inset of Fig. 4. We observed a small sample-dependent shift of these magnetic transition of $\Delta T = \pm 1$ K for the high and $\Delta T = \pm 2$ K for the low transition, when comparing measurements on different single crystals. The Weiss temperatures hint to a dominant antiferromagnetic exchange between the Cu ions of 400 K, but the order appears only below 15 K. Therefore $EuCu_3(OH)_6Cl_3$ is a strongly frustrated system with a frustration coefficient $f = |\vartheta_W|/T_C \approx 30$.

Insight into the nature of the magnetic transition can be obtained from the magnetization curves between 2 and 20 K shown in Fig. 5. A small but well defined hysteresis can be seen for a magnetic field within the kagome plane. However, the spontaneous moment below T_{N_1} is only $0.5 \times 10^{-3}\ \mu_B$ per Cu and $1 \times 10^{-3}\ \mu_B$ below T_{N_2}. This shows that the magnetic order has a tiny in-plane ferromagnetic component. For fields perpendicular to the kagome layers nearly no hysteresis was observed. At higher magnetic fields, both directions present a linear $M(H)$ dependence, with a higher slope for the direction perpendicular to the kagome plane. At 9 T, M reaches only about 0.05 and 0.14 μB/Cu for the two field directions, which is well below the saturation magnetization of 1 μ_B per Cu^{2+} ion. Furthermore, also the Van Vleck contribution from Eu might contribute to the magnetization at higher fields, but is difficult to entangle from the Cu magnetism. For that purpose, a reference compound with Zn instead of Cu would be necessary, which, however, is not known to exist so far.

E. Specific heat

The observed magnetic transitions in the magnetic measurements were also analyzed on several crystals by specific heat. This is essential to exclude contributions from small foreign phases to be the origin of the observed magnetic signals. We show a measurement between 1.8 and 39 K on a single crystal of 8.61 mg. The general specific heat curve divided by temperature is shown in Fig. 6 for a field of 0 and 9 T. We roughly estimated this phonon part in a temperature range 20–32 K from a linear fit of C/T versus T^2 plot. With $\beta = 0.625(6)$ mJ/mol, we get an estimated Debye temperature of $\Theta_D \approx 390$ K slightly above the one of $Y_3Cu_9(OH)_{19}Cl_8$ [9]. We notice that this estimate is very rough and only used to show an order of magnitude for the phonon contribution. The reason is apparent from Fig. 6, because also at 30 K a clear T^3 dependance of the specific heat is not obtained, due to magnetic contributions from the fluctuating moments, hindering a more accurate fit of the phonon contribution. At 15 K, we observe a broad peak in the specific heat data, proving

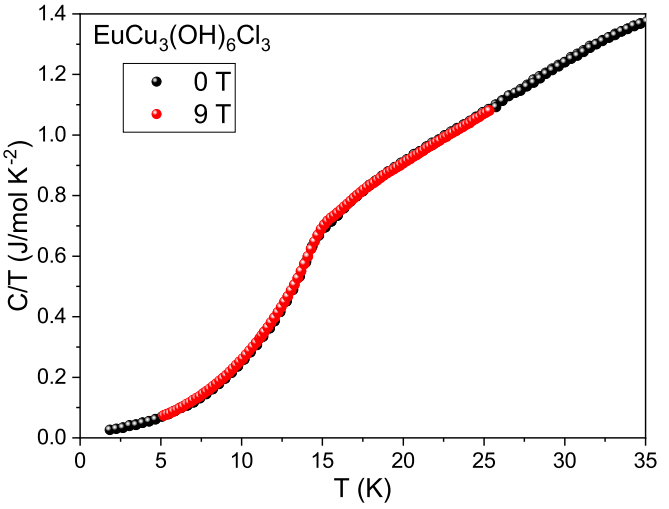

FIG. 6. Specific heat measurements of $EuCu_3(OH)_6Cl_3$ in 0 and 9 T perpendicular to the kagome plane measured from 1.8 to 39 K on a single crystal of 8.61 mg. A broad anomaly is visible at the magnetic ordering temperature.

TABLE III. Results of substitution amounts obtained by EDS analysis on single crystals of different batches prepared with different molar amounts of $Zn(NO_3)_2$. The error for x_{Zn} is a statistical one, obtained by measuring several spots on several crystals from the same batch.

$Zn(NO_3)_2 \cdot 6\,H_2O$ (g)	2	2.5	3	4
$\langle x_{Zn} \rangle$	0.32(9)	0.50(12)	0.61(9)	0.86(4)

that the transition observed in the magnetic measurements is an intrinsic property of $EuCu_3(OH)_6Cl_3$. This transition shows no field dependance for fields up to 9 T. This is in line with the $M(H)$ curve up to 9 T, where no saturation was reached, showing that the field scale of 9 T is far below the energy scale of the dominant magnetic coupling. The entropy connected with the small peak is well below the full ordered moment of Cu, in agreement with the large frustration coefficient found in the magnetic measurements.

IV. $Zn_xCu_{4-x}(OH)_6(NO_3)_2$

A. Synthesis

Powder samples of $ZnCu(OH)_6(NO_3)_2$ were prepared by a solid state reaction of 0.337 g ZnO with 1g $Cu(NO_3)_2 - 6\,H_2O$ and 0.6585 g CuO sealed in a Parr 4749 acid digestion vessel heated to 220 °C for two days then rapidly cooled to room temperature.

Single crystals of $Zn_xCu_{4-x}(OH)_6(NO_3)_2$ were prepared in the Parr autoclave with a temperature profile adapted from the optimized one from $Y_3Cu_9(OH)_{19}Cl_8$ [9]. For the crystallization, we placed duran glass ampoules filled with the solution in the autoclave and filled it with distilled water to ensure the same pressure as in the ampoules. The ampoules were loaded with 0.4 g CuO and 2–4 g $Zn(NO_3)_2 \cdot 6H_2O$ (see Table III) solved in 3 ml distilled water and then sealed at air. The autoclave was heated up to 270 °C in four hours and subsequently cooled down to 140 °C with 1.4 K/h, followed by a fast cooling to room temperature. Afterwards, the ampoules were opened and the content was filtered with distilled water. The ampoules contained a few larger single crystals, some smaller ones and a pellet. The crystals have blue color and a square shape with typical sizes up to $1 \times 1 \times 0.25$ mm^3, where some are depicted in Fig. 7.

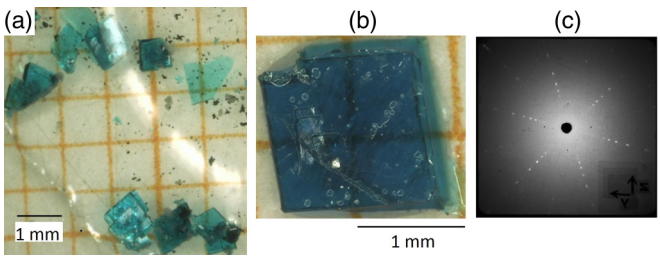

FIG. 7. [(a) and (b)] Picture of $ZnCu_3(OH)_6(NO_3)_2$ crystals from a hydrothermal growth by slow cooling. (c) Laue image of the crystal depicted in (b).

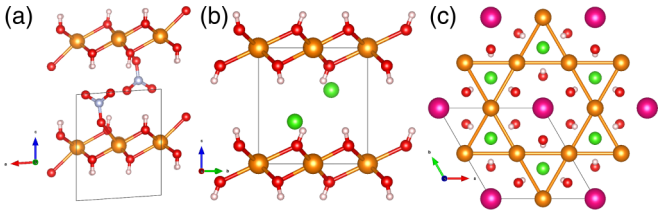

FIG. 8. (a) Picture of the $Zn_xCu_{4-x}(OH)_6(NO_3)_2$ structure viewed along the b axis. (b) Picture of the haydeeite structure viewed along the a axis. The color code is A = Zn, Cu, Mg (orange), O (red), Cl (green), N (grey), and H (white). (c) Picture of the haydeeite structure viewed along the c axis now with Mg in pink.

B. EDS analysis

We measured EDS spectra on several crystals of different batches with different molar amounts of $Zn(NO_3)_2$. For this compound, a considerable intensity is only caused by Zn, Cu, and O and we found a stoichiometry $Zn_xCu_{4-x}(OH)_6(NO_3)_2$ with a variation of the Zn to Cu ratio, depending on the initial content of $Zn(NO_3)_2$ in the solution. Some examples of the substitution amount versus $Zn(NO_3)_2$ amount are given in Table III, which show a nearly linear increase controlled by the molar ratio, similar to herbertsmithite, where a strong excess of Zn^{2+} ions is necessary to reach substitutions of $x = 1$.

C. Structure

From Table I it can be seen that presently two variants in that family with the NO_3 anion were reported in literature. Rouaite, $Cu_4(OH)_6(NO3)_2$, with space group $P2_1$ and $CdCu_3(OH)_6(NO_3)_2$ with space group $P\bar{3}m1$ similar to haydeeite. It is difficult to differentiate Zn and Cu from x rays, thus we found the structure of rouaite as the supergroup $P2_1$ (No. 4) to be the correct cell by taking only Cu atoms on the Zn-Cu positions, $A_4(OH)_6(NO_3)_2$ with A = Zn, Cu [52]. The structure generally describes the matrix and was obtained by single-crystal diffraction. To envision the similarities in Fig. 8, the structure is shown along the b axis compared to the a axis of haydeiite with Mg changed to Cu as it is chosen for the $P2_1$ structure. From the image, one can easily see the similar arrangement of the A ions and the comparable positions of Cl and NO_3. Thus a similar structure is expected for $Zn_xCu_{4-x}(OH)_6(NO_3)_2$, as depicted in Fig. 8(c). To differentiate between Zn and Cu, resonant x rays are necessary to find the correct subgroup.

The distances are $d_{A\text{-}A} = 3.0648(4)$ Å of the Cu atoms in the kagome plane and $d_{A\text{-}A} = 6.9271(9)$ Å between the AA stacked planes. The angle for the dominant superexchange is $\angle$(Cu1-O1-Cu1) = 104.07(12)°. The atomic positions are given in Table IV.

D. Magnetic susceptibility

We performed magnetic measurements on various $Zn_xCu_{4-x}(OH)_6(NO_3)_2$ single crystals. We found that for concentrations $0.3 < x < 0.9$, the magnetic behavior and the ordering temperature are only slightly changed with varying x. In Fig. 9, we show a representative measurement on a single crystal with $x = 0.6$. The overall anisotropy is very

TABLE IV. Structural table obtained by refining (occupation fixed to 1) the single-crystal diffraction data on a $Zn_{0.7}Cu_{3.3}(OH)_6(NO_3)_2$ single crystal measured at 173 K. Using the monoclinic $P2_1$ (No. 4) structure with a unit cell of $a = 5.5704(6)$ Å, $b = 6.1274(7)$ Å, and $c = 6.9271(8)$ Å, $\alpha = \gamma = 90°$, $\beta = 93.782(9)°$.

	x/a	y/b	z/c	Occ.	U_{iso}	Site	Sym.
A1	0.49908	0.50073	0.49403	1	0.007	2a	1
A2	−0.01041	0.25265	0.50224	1	0.007	2a	1
O1	0.3664	0.7556	0.3577	1	0.009	2a	1
H1	0.384	0.773	0.240	1	0.014	2a	1
O2	0.8141	0.5099	0.3755	1	0.008	2a	1
H2	0.819	0.513	0.255	1	0.012	2a	1
O3	0.1877	0.4984	0.6212	1	0.009	2a	1
H3	0.194	0.483	0.743	1	0.013	2a	1
O4	0.2937	0.2596	0.2789	1	0.013	2a	1
O5	0.1092	0.1561	0.0086	1	0.031	2a	1
O6	0.4036	0.3871	0.0063	1	0.026	2a	1
N1	0.2680	0.2675	0.0942	1	0.015	2a	1

small, as can be seen from the magnetization at 2 K up to 9T, where both curves for field parallel and perpendicular to the kagome completely overlap. The susceptibility at 0.1 T shows a well-defined anomaly at $T_N \approx 7.5$ K indicating the onset of antiferromagnetic order. The field dependence of the susceptibility below T_N shows a small anisotropy for magnetic fields below 3 T, this is also reflected in small metamagetic transitions in $M(H)$ in this field range.

From a $\sqrt{\chi T}$ plot (not shown), the effective moment values of $\mu_{\text{eff}}^{||} = 1.62\,\mu_B$ and $\mu_{\text{eff}}^{\perp} = 1.65\,\mu_B$ at 350 K can be derived. A Curie-Weiss fit of the $x = 1$ powder sample is shown in Fig. 9(b) and a Curie-Weiss temperature of $\Theta_W \approx 5$ K is obtained, which indicates contributions both from ferromagnetic and antiferromagnetic exchange couplings.

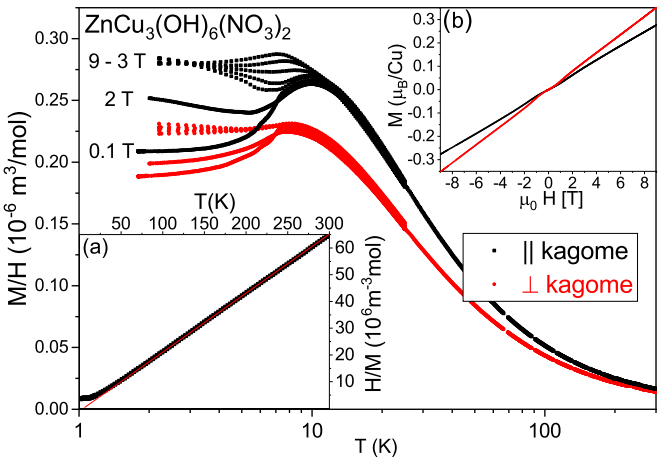

FIG. 9. The image shows the magnetic data on a $Zn_{0.6}Cu_{3.4}(OH)_6(NO_3)_2$ single crystal with a mass of 2.23 mg of the susceptibility in the range of 1.8–350 K field cooled at 0.1–9 T with the field aligned (black dots) and perpendicular to the kagome plane (red dots). (a) Inverse susceptibility $(M/H)^{-1}$ measured on a powder sample of 49.1 mg. (b) $M(H)$ curve at 2 K for both field directions, which lay nearly perfectly on each other.

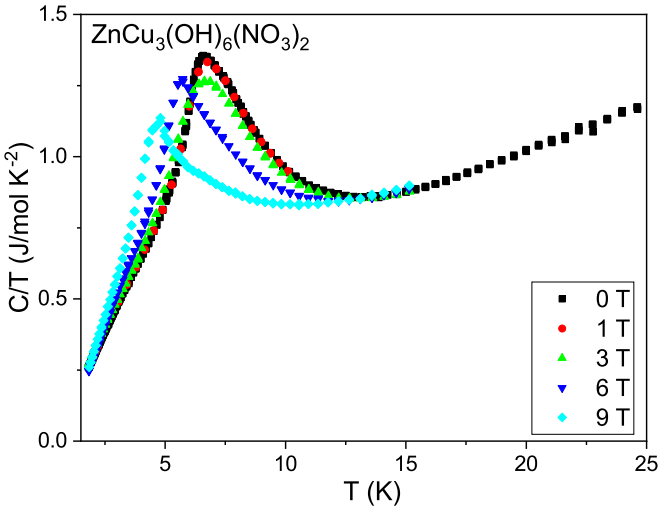

FIG. 10. Specific heat measurements in an external field perpendicular to the plane of 0, 1, 3, 6, and 9 T from 1.8 to 25 K on a single crystal of 5.1 mg. A clear anomaly is visible at the magnetic ordering temperature.

The $M(H)$ curve above 3 T reveals nearly perfect linear behavior with a polarized moment of about 0.3 μ_B at 9 T, still well below the saturated moment of 1 μ_B per Cu^{2+}. The overall shape of the $M(H)$ curve confirms the antiferromagnetic nature of the ordered state.

E. Specific heat

We measured the magnetic transition on a single crystal by specific heat. Shown is a measurement within 1.8 and 15 K on a single crystal with $x = 0.6$ and a mass of 8.61 mg. The specific heat curve divided by temperature is shown in Fig. 10 for fields from 0 up to 9 T. We roughly estimated the phonon part in a temperature range of 15–25 K from a linear fit of a C/T versus T^2 plot. With $\beta = 0.800(6)$ mJ/mol, we get an estimated Debye temperature of $\Theta_D \approx 387$ K. We observe a pronounced peak at T_N, which is slowly shifted to lower temperatures with increasing fields and reaches 5 K at 9 T. The ordered fraction connected to the anomaly is much higher, compared to the $EuCu_3(OH)_6Cl_3$ system and proves that $ZnCu(OH)_6(NO_3)_2$ is only slightly geometrically frustrated, which is in agreement with the small frustration coefficient from the magnetic data.

V. $MgCu_3(OH)_6Cl_2$

A. Synthesis

So far, reports on the synthesis of haydeeite powder samples were only on a reflux setup with oxygen flushing [37]. Here, we present a simple way to produce polycrystalline haydeeite $MgCu_3(OH)_6Cl_2$ samples using a reaction of 1 g $MgCl_2 \cdot 4\,H_2O$ and 1.16 g CuO heated to 220 °C for three days in a Parr 4749 acid digestion vessel. The synthesis is enabled due to the low dissociation temperature of $MgCl_2 \cdot 4\,H_2O$ at 110 °C. Single crystals could then be prepared by the external gradient method using the prereacted powder as a starting material being dissolved in a solution of 6 g $MgCl_2 \cdot 4\,H_2O$ and 5 ml distilled water. The solution was optimized by another

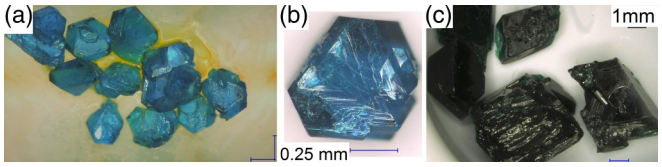

FIG. 11. [(a) and (b)] Picture of haydeeite crystals grown in an external gradient. (c) Images of the parasitic tondiite crystals which dominantly grow below 180 °C.

prereaction method of 6 g $MgCl_2 \cdot 4H_2O$ dissolving 0.48 g CuO in 5 ml water at 220 °C for three days leading up to 100-μm haydeeite crystals. It turned out that the temperature window for the crystallization of haydeeite is narrow. We found 180 °C to be the optimal temperature at the cold end, since the polymorphic tondiite $Mg_xCu_{4-x}(OH)_6Cl_2$ crystals are formed during the synthesis below 180 °C. These tondiite crystals grow even up to 100 mg with $4 \times 4 \times 3$ mm^3 [see Fig. 11(c)]. However, they have an extremely low substitution amount of Mg ($0.05 < x < 0.4$) due to the high $MgCl_2$ concentration being optimized for haydeeite. Similar to herbertsmithite, higher $MgCl_2$ concentrations lead to a decreased Mg content in the formed tondiite crystals. With a gradient of 200 °C–180 °C in a 15-cm ampoule we succeeded to grow hexagonal blue single crystals of up to $0.5 \times 0.5 \times 0.25$ mm^3 and 1.6 mg depicted in Figs. 11(a) and 11(b).

B. EDS analysis

We measured EDS in the SEM on several crystals of different batches and found a rather high uncertainty for Mg-Cu with this method. To get a grasp of the Mg content, we performed electron probe microanalysis (EPMA) on up to four crystals of two different batches. We found an enhanced average substitution content of $x_{\mathrm{Mg}} = 1.2 \pm 0.2$, compared to even stronger enhanced values with $x_{\mathrm{Mg}} = 1.49 \pm 0.16$ reported in Ref. [37].

C. Magnetic susceptibility

Magnetic and neutron scattering experiments on polycrystalline haydeeite revealed a ferromagnetic ground state below $T_C = 4.2$ K [37,56]. Here, we present the magnetic measurements on a single crystal with a mass of 0.3 mg. The susceptibility shown in Fig. 12 was measured both along and perpendicular to the kagome plane and reveals a small anisotropy below T_C. The sample shows a ferromagnetic order around 4.31 K with a sizable field dependence stabilizing the magnetic order as expected for a ferromagnet. From a $\sqrt{\chi T} \sim \mu_{\mathrm{eff}}$ plot shown in the inset of Fig. 12 the effective moment value of $\mu_{\mathrm{eff}} = 1.9\,\mu_B$ at 290 K can be derived.

The magnetization curve in the ordered phase at 1.9 K shown in Fig. 13 confirms the ferromagnetic nature of the transition. We observe an ordered moment of $M_s = 1$ μB for both field directions, with the easy axis within the kagome plane, where the saturation is reached around 0.1 T. For field perpendicular to the kagome plane, the critical field is around 2 T. We were not able to resolve a finite hysteresis curve properly. We note that the ordered moment is larger than reported in Refs. [51,56], there an ordered moment of

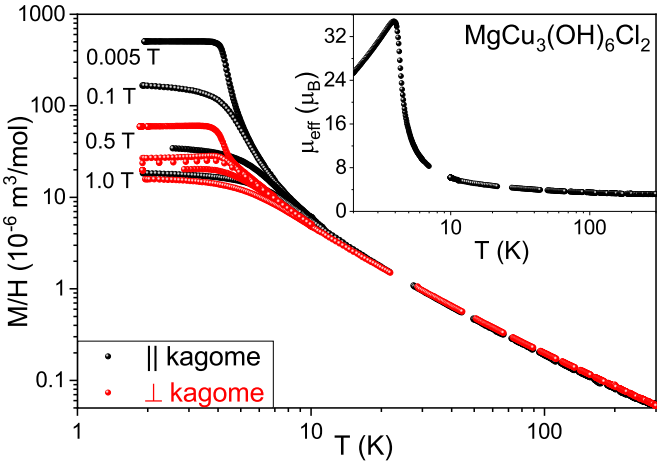

FIG. 12. The image shows the magnetic data on a $MgCu_3(OH)_6Cl_2$ single crystals with a mass of 1.6 mg of the susceptibility in the range of 1.8–300 K field cooled at 0.1–1 T with the field aligned parallel (red dots) and perpendicular to the kagome plane (black dots). The main figure shows a log-log plot of the temperature-dependent susceptibility at various fields. The inset is a rescaling on the effective moment by a $\sqrt{\chi T}$ plot of the 50 Oe curve.

0.28 mB (at 500 Oe) and $M_s = 0.83$ mB per mole of Cu, was reported. The reason might be the slightly different x values. A Curie-Weiss fit of a stack of single crystals for a field applied parallel to the kagome plane is shown in the inset of Fig. 13(c) and yields Curie-Weiss temperatures of $\Theta_W^{||} = 26$ K compared to $\Theta_W = 28 \pm 3$ K for powder data [56].

D. Specific heat

The observed magnetic transition was also analyzed on several crystals by specific heat. In Fig. 14, we show a measurement between 1.8 and 20 K on a single crystal of 0.3 mg. The specific heat curve divided by temperature is shown in Fig. 14 for fields of 0, 0.1, 0.5, 1, 2, 3, and 4 T along

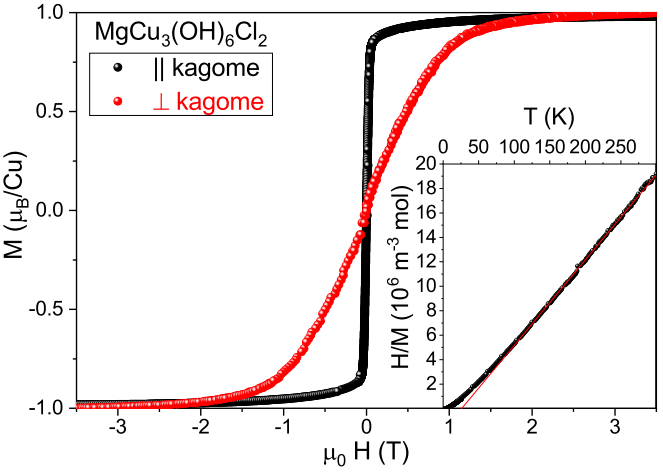

FIG. 13. Field-dependent magnetization measured at 1.9 K for both field directions parallel (black) and perpendicular (red) to the kagome plane. The inset shows the inverse susceptibility H/M of a stack of single crystals of 1.6 mg plotted vs temperature at a field of 0.1 T applied parallel to the kagome plane.

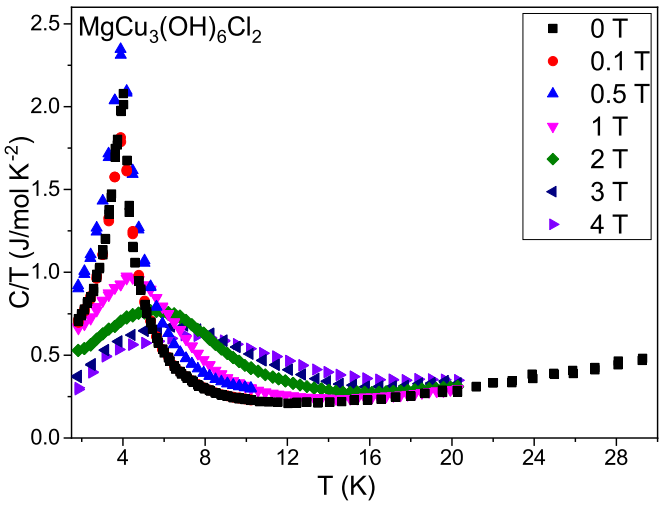

FIG. 14. Specific heat measurements in an external field of 0, 0.1, 0.5, 1, 2, 3, and 4 T applied perpendicular to the kagome plane, measured from 1.8 to 20 K on a single crystal of 0.3 mg.

the kagome plane. We roughly estimated the contributions in a temperature range of 15–32 K from a linear fit of a C/T versus T^2 plot. With $\beta \approx 0.402(7)$ mJ mol^{-1} K^{-2} we get an estimated Debye temperature of $\Theta_D \approx 443$ K. We observe a sharp peak at the magnetic transition, which can best be seen in the C/T plot in Fig. 14, which shows a strong field dependence shifting it up to 10 K at 4 T. The increased area under the peak compared to the two previously shown compounds is in agreement with the full captured moment in the $M(H)$ curve.

VI. CONCLUSION

In conclusion, we have presented results on three members of two-dimensional kagome quantum spin systems in the atacamite family. The successful hydrothermal synthesis of single crystals for these three candidates has been shown. They reveal very different magnetic ground states. $EuCu_3(OH)_6Cl_3$ is a kapellasite-like kagome material with the highest reported Curie-Weiss temperature for the atacamite family of -400 K and presents the strongest anisotropy in this family of up to 2.7 due to Van Vleck paramagnetic Eu^{3+} contributions. The system is strongly frustrated with partial order at 14.7 K and a spin reorientation at 8.7 K. The frustration coefficient is around 30. $ZnCu_3(OH)_6(NO_3)_2$ turned out to be an antiferromagnetic system without strong frustration effects. Magnetic measurements on single crystals revealed only tiny anisotropy in this compound. Furthermore, we present measurements on single crystals of haydeeite and confirmed the ferromagnetic order at 4.3 K measured previously on polycrystals. We detect a small but well-defined anisotropy in the ordered phase with the easy axis within the kagome plane. In addition, the specific-heat measurements reveal a clear anomaly, confirming the absence of sizable frustration effects.

These results together with a compilation of the physical and structural properties of kagome materials around the atacamite family shows us a rich playground where the perfect spin liquid candidate is in close reach. The clue to the latter might be in a more in-depth study of the delicate interplay of the different magnetic exchange couplings. The materials presented in this study give a firm basis to study this influence on the overall degree of frustration in kagome quantum spin systems. Finally, from the presented kagome systems and the listed ones, one can assume that an increasing separation of the kagome plane does not stabilize the spin liquid properties.

ACKNOWLEDGMENT

The authors gratefully acknowledge support by the Deutsche Forschungsgemeinschaft through Grant No. SFB/TR 49.

[1] L. Balents, Spin liquids in frustrated magnets, Nature (London) **464**, 199 (2010).

[2] M. P. Shores, E. A. Nytko, B. M. Barlett, and D. G. Nocera, A structurally perfect S = (1/2) kagomé antiferromagnet, J. Am. Chem. Soc. **127**, 13462 (2005).

[3] J. S. Helton, K. Matan, M. P. Shores, E. A. Nytko, B. M. Bartlett, Y. Yoshida, Y. Takano, A. Suslov, Y. Qiu, J.-H. Chung, D. G. Nocera, and Y. S. Lee, Spin Dynamics of the Spin-1/2 Kagome Lattice Antiferromagnet $ZnCu_3(OH)_6Cl_2$, Phys. Rev. Lett. **98**, 107204 (2007).

[4] P. Mendels, F. Bert, M. A. de Vries, A. Olariu, A. Harrison, F. Duc, J. C. Trombe, J. S. Lord, A. Amato, and C. Baines, Quantum Magnetism in the Paratacamite Family: Towards an Ideal Kagomé Lattice, Phys. Rev. Lett. **98**, 077204 (2007).

[5] M. A. de Vries, D. Wulferding, P. Lemmens, J. S. Lord, A. Harrison, P. Bonville, F. Bert, and P. Mendels, Extension of the zinc paratacamite phase diagram: Probing the effect of spin vacancies in an S = 1/2 kagome antiferromagnet, Phys. Rev. B **85**, 014422 (2012).

[6] T.-H. Han, M. R. Norman, J.-J. Wen, Jose A. Rodriguez-Rivera, Joel S. Helton, Collin Broholm, and Young S. Lee, Correlated impurities and intrinsic spin-liquid physics in the kagome material herbertsmithite, Phys. Rev. B **94**, 060409(R) (2016).

[7] M. R. Norman, Colloquium: Herbertsmithite and the Search for the Quantum Spin Liquid, Rev. Mod. Phys. **88**, 041002 (2016).

[8] I. I. Mazin, H. O. Jeschke, F. Lechermann, H. Lee, M. Fink, R. Thomale, and R. Valentí, Nat. Commun. **5**, 4261 (2014).

[9] P. Puphal, M. Bolte, D. Sheptyakov, A. Pustogow, K. Kliemt, M. Dressel, M. Baenitz, and C. Krellner, Strong magnetic frustration in $Y_3Cu_9(OH)_{19}Cl_8$: A distorted kagome antiferromagnet, J. Mater. Chem. C **5**, 2629 (2017).

[10] W. Sun, Y. Huang, S. Nokhrin, Y. Pan, and J. Mi, Perfect Kagomé lattices in $YCu_3(OH)_6Cl_3$: A new candidate for the quantum spin liquid state, J. Mater. Chem. C **4**, 8772 (2016).

[11] W. Sun, Ya-Xi Huang, Y. Pan, and J. Mi, Strong spin frustration and negative magnetization in $LnCu_3(OH)_6Cl_3$ (Ln = Nd and Sm) with triangular lattices: The effects of lanthanides, Dalton Trans. **46**, 9535 (2017).

[12] H. R. Oswald and W. Feitknecht, Über die Hydroxidhalogenide $Me_2(OH)_3Cl$, -Br, -J zweiwertiger Metalle (Me = Mg, Ni, Co, Cu, Fe, Mn), Helv. Chim. Acta **47**, 272 (1964).

[13] T.-T. Zhu, W. Sun, Y.-X. Huang, Z.-M. Sun, Y. Pan, L. Balents, and J.-X. Mi, Strong spin frustration from isolated triangular Cu(II) trimers in $SrCu(OH)_3Cl$ with a novel cuprate layer, Mater. Chem. C **2**, 8170 (2014).

[14] Y. Li, B. Pan, S. Li, W. Tong, L. Ling, Z. Yang, J. Wang, Z. Chen, Z. Wu, and Q. Zhang, Gapless quantum spin liquid in the $S = 1/2$ anisotropic kagome antiferromagnet $ZnCu_3(OH)_6SO_4$, New J. Phys. **16**, 093011 (2014).

[15] R. D. Shannon and C. T. Prewitt, Effective Ionic Radii in Oxides and Fluorides, Acta Crystallogr. B **25**, 925 (1969).

[16] R. D. Shannon, Revised Effective Ionic Radii and Systematic Studies of Interatomie Distances in Halides and Chaleogenides, Acta Crystallogr. A **32**, 751 (1976).

[17] H. D. B. Jenkins and K. P. Thakur, Reappraisal of Thermochemical Radii for Complex Ions, J. Chem. Educ. **56**, 576 (1979).

[18] X. G. Zheng, T. Mori, K. Nishiyama, W. Higemoto, H. Yamada, K. Nishikubo, and C. N. Xu, Antiferromagnetic transitions in polymorphous minerals of the natural cuprates atacamite and botallackite $Cu_2Cl(OH)_3$, Phys. Rev. B **71**, 174404 (2005).

[19] X. G. Zheng, T. Kawae, Y. Kashitani, C. S. Li, N. Tateiwa, K. Takeda, H. Yamada, C. N. Xu, and Y. Ren, Unconventional magnetic transitions in the mineral clinoatacamite $Cu_2Cl(OH)_3$, Phys. Rev. B **71**, 052409 (2005).

[20] S. Chu, P. Müller, D. G. Nocera, and Y. S. Lee, Hydrothermal growth of single crystals of the quantum magnets: Clinoatacamite, paratacamite and herbertsmithite, Appl. Phys. Lett. **98**, 092508 (2011).

[21] S. Vilminot, M. Richard-Plouet, G. André, D. Swierczynski, F. Bourée-Vigneron, and M. Kurmooc, Nuclear and magnetic structures and magnetic properties of synthetic brochantite, $Cu_4(OH)_6SO_4$, Dalton Trans. **0**, 1455 (2006).

[22] Emily A. Nytko, *Synthesis, structure, and magnetic properties of spin-1/2 kagomé antiferromagnets*, PhD. thesis, MIT, 2008.

[23] H. Effenberger, Verfeinerung der Kristallstruktur des monoklinen Dikupfer(II)-trihydroxi-nitrates $Cu_2(NO_3)(OH)_3$, Zeitschrift für Kris **165**, 127 (1983).

[24] P. C. Burns, M. A. Cooper, and F. C. Hawthorne, Claringbullite; a Cu^{2+} oxysalt with Cu^{2+} in trigonal-prismatic coordination, Burns The Canadian Mineralogist **33**, 633 (1995).

[25] T.-H Han, J. Singleton, and J. A. Schlueter, Barlowite: A Spin-1/2 Antiferromagnet with a Geometrically Perfect Kagome Motif, Phys. Rev. Lett. **113**, 227203 (2014).

[26] P. Elliott, M. A. Cooper, and A. Pring, Barlowite, $Cu_4FBr(OH)_6$, a new mineral isostructural with claringbullite: Description and crystal structure, Mineral. Mag. **78**, 1755 (2014).

[27] C. M. Pasco, B. A. Trump, Thao T. Tran, Z. A. Kelly, C. Hoffmann, I. Heinmaa, R. Stern, and T. M. McQueen, Single crystal growth of $Cu_4(OH)_6Br_F$ and universal behavior in quantum spin liquid candidates synthetic barlowite and herbertsmithite, Phys. Rev. Mater. **2**, 044406 (2018).

[28] M. D. Welch, M. J. Sciberras, P. A. Williams, P. Leverett, J. Schlüter, and T. Malcherek, A temperature-induced reversible transformation between paratacamite and herbertsmithite, Phys. Chem. Min. **41**, 33 (2014).

[29] Pascal Puphal, Ranjith Kumar, Max Muller, Edwin Kermarrec, Denis Sheptyakov, Fabrice Bert, Michael Baenitz, Philippe Mendels, and Cornelius Krellner, $GaxCu_{4-x}(OD)_6Cl_2$: Insulating ground state in an electron-doped kagome system (unpublished).

[30] Y.-S. Li and Q.-M. Zhang, Structure and magnetism of $S = 1/2$ kagome antiferromagnets $NiCu_3(OH)_6Cl_2$ and $CoCu_3(OH)_6Cl_2$, J. Phys.: Condens. Matter **25**, 026003 (2013).

[31] M. E. Clissold, P. Leverett, P. A. Williams, D. E. Hibbs, and E. H. Nickel, The structure of gillardite, the Ni-analogue of herbertsmithite, from Widgiemooltha, western Australia, Canadian Min. **45**, 317 (2007).

[32] S. Chu, T. M. McQueen, R. Chisnell, D. E. Freedman, P. Müller, Y. S. Lee, and D. G. Nocera, A $Cu^{2+}(S = 1/2)$ Kagomé Antiferromagnet: $Mg_xCu_{4-x}(OH)_6Cl_2$, J. Am. Chem. Soc. **132**, 5570 (2010).

[33] K. Mereiter, Herbertsmithite, $Cu_3Zn(OH)_6Cl_2$, from Mina Los Tres Presidentes, Sierra Gorda, Chile, refinement based on CCD diffractometer data (private communication).

[34] Zili Feng, Yuan Wei, Ran Liu, Dayu Yan, Yan-Cheng Wang, Jianlin Luo, Anatoliy Senyshyn, Clarina dela Cruz, Wei Yi, Jia-Wei Mei, Zi Yang Meng, Youguo Shi, and Shiliang Li, Effect of Zn doping on the antiferromagnetism in kagome $Cu_{4-x}Zn_x(OH)_6FBr$, arXiv:1712.06732v1.

[35] A. R. Kampf, M. J. Sciberras, P. A. Williams, M. Dini, and A. A. Molina Donoso, Leverettite from the Torrecillas mine, Iquique Provence, Chile: The Co-analogue of herbertsmithite, Mineral. Mag. **77**, 3047 (2013).

[36] T. M. McQueen, T. H. Han, D. E. Freedman, P. W. Stephens, Y. S. Lee, and D. G. Nocera, $CdCu_3(OH)_6Cl_2$: A new layered hydroxide chloride, J. Solid State Chem. **184**, 3319 (2011).

[37] R. H. Colman, A. Sinclair, and A. S. Wills, Comparisons between Haydeeite, α-$Cu_3Mg(OH)_6Cl_2$, and Kapellasite, α-$Cu_3Zn(OH)_6Cl_2$, Isostructural $S = 1/2$ Kagome Magnets, Chem. Mater. **22**, 5774 (2010).

[38] T. Malcherek and J. Schlüter, $Cu_3MgCl_2(OH)_6$ and the bond-valence parameters of the OH-Cl bond, Acta Crystallogr. B **63**, 157 (2007).

[39] R. H. Colman, C. Ritter, and A. S. Wills, Toward Perfection: Kapellasite, $Cu_3Zn(OH)_6Cl_2$, a New Model $S = 1/2$ Kagome Antiferromagnet, Chem. Mater. **20**, 6897 (2008).

[40] D. Nishio– Hamane, K. Momma, M. Ohnishi, N. Shimobayashi, R. Miyawaki, N. Tomita, R. Okuma, A. R. Kampf, T. Minakawa, and M. Rumsey, Iyoite, $MnCuCl(OH)_3$ and misakiite, $Cu_3Mn(OH)_6Cl_2$: New members of the atacamite family from Sadamisaki Peninsula, Ehime Prefecture, Japan, Mineral. Mag. **81**, 485 (2017).

[41] R. Okuma, T. Yajima, D. Nishio-Hamane, T. Okubo, and Z. Hiroi, Weak ferromagnetic order breaking the threefold rotational symmetry of the underlying kagome lattice in $CdCu_3(OH)_6(NO3)_2 \cdot H_2O$, Phys. Rev. B **95**, 094427 (2017).

[42] W. Sun, Y. Huang, Y. Pan, and J. Mi, Synthesis and magnetic properties of centennialite: A new S = ½ Kagomé antiferromagnet and comparison with herbertsmithite and kapellasite, Phys. Chem. Miner. **43**, 127 (2016).

[43] H. Yoshida *et al.*, Unusual Magnetic State with Dual Magnetic Excitations in the Single Crystal of $S = 1/2$ Kagome Lattice Antiferromagnet $CaCu_3(OH)_6Cl_2{\cdot}0.6\ H_2O$, J. Phys. Soc. Jpn. **86**, 033704 (2017).

[44] H. Yang, I. F. Barton, M. B. Andrade, and R. T. Downs, Crystal structure of a new compound, $CuZnCl(OH)_3$, isostructural with botallackite, Am. Mineral. **101**, 986 (2016).

[45] X. G. Zheng, M. Hagihala, K. Nishiyama, and T. Kawae, Exotic antiferromagnetic transition in deformed pyrochlore lattice

$Ni_2(OH)_3Cl$ of atacamite-structure, Phys. B: Cond. Mat. **404**, 677 (2009).

[46] M. Hagihala, X. G. Zheng, T. Toriyi, and T. Kawae, Antiferromagnetism and geometric frustration in tetrahedral lattice hydroxyhalides $M_2(OH)_3X$, J. Phys.: Condens. Matter **19**, 145281 (2007).

[47] J. Rodriguez-Carvajal, Recent advances in magnetic structure determination by neutron powder diffraction, Physica B **192**, 55 (1993).

[48] Stoe and Cie GmbH, X-AREA. *Diffractometer Control Program System* (2002).

[49] G. M. Sheldrick, Acta Crystallogr. A **64**, 112 (2008).

[50] T. H. Han, J. S. Helton, S. Chu, A. Prodi, D. K. Singh, C. Mazzoli, P. Müller, D. G. Nocera, and Y. S. Lee, Synthesis and characterization of single crystals of the spin-1/2 kagome-lattice antiferromagnets $Zn_xCu_{4-x}(OH)_6Cl_2$, Phys. Rev. B **83**, 100402(R) (2011).

[51] R. H. Colman, A. Sinclair, and A. S. Wills, Comparisons between Haydeeite, a-$Cu_3Mg(OD)_6Cl_2$, and Kapellasite, a-$Cu_3Zn(OD)_6Cl_2$, Isostructural $S = 1/2$ Kagome Magnets, Chem. Mater. **23**, 1811 (2011).

[52] See Supplemental Material at http://link.aps.org/supplemental/10.1103/PhysRevMaterials.2.063402 for (1) $EuCu_3(OH)_6Cl_3$ and (2) $ZnCu_3(OH)_6(NO_3)_2$.

[53] M. Tovar, D. Rao, J. Barnett, B. S. Oseroff, J. D. Thomson, S.-W. Cheong, Z. Fisk, D. C. Vier, and S. Schultz, Eu_2CuO_4: An anistropic Vanvleck paramagnet, Phys. Rev. B **39**, 2661 (1989).

[54] Y. Yamaguchi, S. Waki, M. Tokumoto, and K. Hayashi, Crystal-field effect on magnetic susceptibility of $EuBa_2Cu_3O_y$, Solid State Commun. **66**, 1079 (1988).

[55] H. Lueken, *Magnetochemie*, Teubner Stuttgart, Leipzig, 1999.

[56] D. Boldrin, B. Fak, M. Enderle, S. Bieri, J. Ollivier, S. Rols, P. Manuel, and A. S. Wills, Haydeeite: A spin-1/2 kagome ferromagnet, Phys. Rev. B **91**, 220408(R) (2015).